Available online at www.sciencedirect.com
ScienceDirect
Journal of Solid State Chemistry 180 (2007) 221–232
JOURNAL OF SOLID STATE CHEMISTRY
www.elsevier.com/locate/jssc

$Ni_{7-\delta}SnTe_2$: Modulated crystal structure refinement, electronic structure and anisotropy of electroconductivity

A.A. Isaeva[a], A.I. Baranov[b], Th. Doert[c], B.A. Popovkin[d,*], V.A. Kulbachinskii[e], P.V. Gurin[e], V.G. Kytin[e], V.I. Shtanov[d]

[a]Department of Materials Science, Moscow State University, Leninskie Gory, Moscow 119992, GSP-2, Russia
[b]Max Planck Institute for Chemical Physics of Solids, Noethnitzer Strasse, 40, 01187 Dresden, Germany
[c]Institute of Inorganic Chemistry, Dresden University of Technology, 01062 Dresden, Germany
[d]Department of Chemistry, Moscow State University, Leninskie Gory, Moscow 119992, GSP-2, Russia
[e]Department of Physics, Moscow State University, Leninskie Gory, Moscow 119992, GSP-2, Russia

Received 10 April 2006; received in revised form 19 July 2006; accepted 4 September 2006
Available online 15 September 2006

Abstract

Single crystals of $Ni_{7-\delta}SnTe_2$ were grown during re-crystallization of the presynthesized powder in a two zone furnace. The modulated structure was solved and refined in the (3 + 2)-dimensional superspace group $I4/mmm(0–\alpha0,\ \alpha00)0.ss.mm$ with lattice parameters $a = 3.759(1)$ and $c = 19.410(2)$ Å (measured at 153 K) and $Z = 2$. Satellite reflections observed in the diffraction images can be assigned to the incommensurate modulation vectors $\mathbf{q}_1 = da^*$ and $\mathbf{q}_2 = db^*$ with $d = 0.410(1)$. The composition resulting from X-ray structure refinement is $Ni_{5.81}SnTe_2$. The structure model has been also developed in the orthorhombic (3 + 1)-dimensional superspace group $Immm(\alpha00)00s$ assuming twinning according to [110], giving thus the composition $Ni_{5.79}SnTe_2$. The origin of the modulation can be attributed to a variation of the occupancy of the Ni(3) site in Ni/Te slabs of the structure. Band structure calculations on a commensurate approximant and single crystal electrical resistivity measurements reveal anisotropic metallic conductivity for this compound.

Keywords: Metal-rich ternary chalcogenides; Modulated structure; Chemical bonding; Electroconductivity

1. Introduction

In recent years, a new family of crystal phases consisting of alternating heterometallic and metal-chalcogenide slabs was discovered. Among these, $Ni_{5.72(3)}SbSe_2$, $Ni_{5.66(2)}SbTe_2$ [1], $Ni_{5.98(3)}SnS_2$, $Ni_{8.93(1)}Sn_2S_2$ [2], $Ni_{5.62(1)}SnSe_2$, $Ni_{5.78(2)}SnTe_2$ [3] and the solitary palladium analog $Pd_{6.21(1)}SnTe_2$ [4] have to be mentioned. The crystal structures of these compounds are composed of heterometallic $^2_\infty[M_5B]$ (M = Ni, Pd; B = Sn, Sb) or $^2_\infty[Ni_8Sn_2]$ slabs of the Cu_3Au type and metal-chalcogenide $^2_\infty[M_xCh_2]$ (M = Ni, Pd; Ch = S, Se, Te) slabs of distorted NaCl or Li_2O type alternating along the c-axis. All compounds are non-stoichiometric due to one partially occupied metal site of the $^2_\infty[M_xCh_2]$ slabs; the compositions presented were obtained from the crystal structure refinement procedures. While all other structures were solved in space group $I4/mmm$, the modulated structure of the palladium compound $Pd_{6.21(1)}SnTe_2$ was refined in the (3 + 2)-dimensional superspace group $I4/mmm(0–\alpha0,\ \alpha00)0.ss.mm$ with the modulation vectors $\mathbf{q}_1 = da^*$ and $\mathbf{q}_2 = db^*$ with $d = 0.4$ using the superspace formalism [4]. The two-dimensional modulation was assigned to an ordering of vacancies in the Pd rows of the $[Pd_{1.21}Te_2]$ slabs.

Investigations of the X-ray diffraction pattern of $Ni_{5.78}SnTe_2$ reveal, that its structure is also modulated, but only the average crystal structure was reported in an earlier contribution. An anisotropy of the electroconductivity for almost all members of the structure family under consideration was predicted by quantum chemical calculations [2–4] and proved by experiments held on pressed $Ni_{5.62}SnSe_2$ polycrystalline pellets ($\rho_\parallel/\rho_\perp \sim 3$); resistivity measurements on single crystals have not been performed

*Corresponding author. Fax: +7 495 939 0998.
E-mail address: popovkin@inorg.chem.msu.ru (B.A. Popovkin).

0022-4596/$ - see front matter © 2006 Elsevier Inc. All rights reserved.
doi:10.1016/j.jssc.2006.09.003

[3]. We therefore put our efforts on growing suitable crystals of the metal-rich nickel–tin telluride for refining its modulated crystal structure and for electroconductivity measurements along different crystallographic directions. The results are presented in the following.

2. Experimental

2.1. Crystal growth

A special quartz ampoule consisting of two interconnected cylindrical chambers with internal diameters 30 and 10 mm, respectively, was used for the crystal growth experiment (see Fig. 1). The height of the bigger chamber was restricted to 10 mm by flat walls. A quartz rod was soldered to the center of the bottom to provide a cold spot region. In total, 1 g of $Ni_{5.78}SnTe_2$ powder (phase pure according to the X-ray powder diagrams and prepared according to the synthetic route reported in [3]) and 0.1 g of iodine were deposited at the bottom of the wide chamber. The container was then evacuated (10^{-2} mmHg) and sealed so that the height of the narrow chamber was 30 mm. The second chamber was topped with a quartz rod for the adjustment of the container's position in a vertical furnace. Finally, the ampoule was positioned in a furnace with small temperature difference between T_1 (wide chamber bottom) and T_2 (narrow chamber top) which was changed during the experiment. At first the ampoule was kept at $T_1 = 635\,^{\circ}C/T_2 = 638\,^{\circ}C$ for 3 days in order to clear its top from crystal nuclei. Then the experimental conditions were changed as follows: $T_1 = 638\,^{\circ}C/T_2 = 624\,^{\circ}C$ for 7 days, then $T_1 = 670\,^{\circ}C/T_2 = 628\,^{\circ}C$ for 6 days and finally $T_1 = 720\,^{\circ}C/T_2 = 699\,^{\circ}C$ for 18 days. No noticeable mass transfer to the narrow chamber was observed at any temperature regime, but the initial sample recrystallized and well-shaped gold-colored platelets ($1.5 \times 1 \times 0.05\,mm^3$) formed inside the sintered sample. The results of EDX analysis (Table 1) correspond with the composition previously obtained from the X-ray structure determination of the average structure [3].

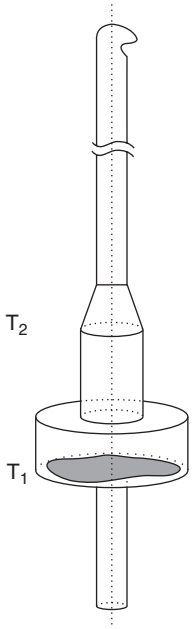

Fig. 1. Ampoule geometry used for $Ni_{7-\delta}SnTe_2$ crystal growth.

Table 1
EDX results (CAMEBAX SX-50, acc. voltage 15 kV, coll. time 100 s)

Element	Calc. (at%)	Exp. (at%)
Ni	65.8	64.6
Sn	11.4	11.9
Te	22.8	23.5
Overall composition	$Ni_{5.78}SnTe_2$	$Ni_{5.42(12)}SnTe_{1.97(1)}$

2.2. Crystal structure investigation

A single crystal was mounted on an image plate diffractometer (STOE IPDS-2, Mo$K\alpha$ radiation, graphite monochromator) and complete data sets were recorded at 293 and 153 K. Integration of the data, as well as Lorenz- and polarization factor corrections were performed with the IPDS software package [5]; a numerical absorption correction was applied based on the refined crystal shape using the STOE X-RED and X-SHAPE software [6]. Lattice parameters and modulation vectors $\mathbf{q}_1$ and $\mathbf{q}_2$ were determined and refined with the IPDS software package [5]. Full-matrix least-squares structure refinements were carried out with JANA2000 against F^2 [7], extinction effects were corrected according to Becker and Coppens [8]. The X-ray data sets recorded at 293 and 153 K reveal no discrepancies, the modulation vectors remain unchanged in this temperature interval and the intensities of the satellites do not increase significantly at lower temperatures. Thus, only the low-temperature data are considered here. The graphical representations of the average and modulated structures were made with DIAMOND [9].

2.3. Electronic structure and bonding

The band structure of the model compound $Ni_{5.75}SnTe_2$ was calculated with the CRYSTAL98 [10] program package. Hay–Wadt effective core potentials (ECPs) and valence basis set [11] were used. The basis set was not optimized, but modified to be used in the calculation of solids in accordance with the recommendations of CRYSTAL98 manual. The basis set (available as Supplementary Material) was tested in the calculations of metals and nickel tellurides and was found suitable for an adequate representation of the main features of their electronic structures and bonding. B3LYP-Hamiltonian was employed in the calculations [12], the convergence criterion for the SCF energy was set to 10^{-7} Hartree.

2.4. Electrical measurements

Single crystals of a typical size $1.5 \times 1 \times 0.05\,mm^3$ were extracted from the sample. Preliminary tests of the crystal orientation on a diffractometer showed the crystallographic *c*-axis to be oriented perpendicular to the largest face of the platelets. The resistivity in the plane of the platelike crystals, i.e. in the crystallographic *ab* plane (in the following called in-plane resistivity and denoted as $\rho_{\perp}$) was measured in two perpendicular directions ($\rho_{1\perp}$ and $\rho_{2\perp}$) by the conventional four-probe method. Contacts were attached to the side faces of the crystal by Wood's alloy using micro-soldering iron. For measuring the resistivity parallel to the *c*-axis (denoted as $\rho_{||}$), the in-plane contacts were removed and four new contacts (two on the upper flat surface of the crystal and two on the lower surface) were used. In both cases two opposite symmetrically placed contacts were used for current supply and two others as potential probes. The temperature dependencies of the electroconductivity were registered in the range from 4 to 300 K.

The Hall effect was measured at liquid helium temperature in a magnetic field up to 6 T with the field oriented parallel to the *c*-axis of the crystal; the current was employed in perpendicular direction.

3. Results and discussion

3.1. Crystal structure determination

The X-ray diffraction image of the crystal exhibits Laue symmetry 4/*mmm*. The lattice parameters were determined to $a = b = 3.759(1)$ and $c = 19.410(2)$ Å at 153 K from the main reflections. Satellite reflections can be observed along the crystallographic *a* and *b* axes. The diffraction images can either be described by a two-dimensional modulation based on a tetragonal unit cell with modulation vectors $\mathbf{q}_1 = d\mathbf{a}^*$ and $\mathbf{q}_2 = d\mathbf{b}^*$ with $d = 0.410(1)$ or by a one-dimensional modulation based on an orthorhombic cell (*a*, $b \approx a$, *c*) and a modulation vector $\mathbf{q} = d\mathbf{a}^*$ with $d = 0.410(1)$ and twinning according to [110].

Selected area electron diffraction (SAED) patterns of a crystal of the composition $Ni_{5.78}SnTe_2$ along [001]*, [$\bar{1}$01]* and [$\bar{4}$01]* have been reported in a previous contribution [3]. The main reflections obey tetragonal *I*4/*mmm* symmetry. In the [001]* SAED pattern no satellites are visible. By tilting the respective crystal around *b**, the [$\bar{1}$01]* and [$\bar{4}$01]* SAED patterns were generated. These diffraction images show weak first order satellites which can be attributed to a modulation vector $\mathbf{q} \approx 0.4\mathbf{b}^*$ (the attentive reader may have noticed, that the assignment of the modulation vector in [3] is not consistent with the indices of the main reflection in the diffraction images displayed in the figure). By tilting the crystal around *b**, satellites running along *a** cannot be depicted as they will coincide with main reflections. No higher-order satellites are visible in the SAED patterns.

Presuming tetragonal symmetry, the reflection conditions of the X-ray data are consistent with the (3 + 2)-dimensional superspace groups *I*4/*mmm*(0–α0, α00)00*mm* and *I*4/*mmm*(0–α0, α00)0.*ss.mm*, in the latter, only reflections *hk*0*mn* with $m + n = 2n$ can be observed [13]. This would explain why no 1st order satellites are found in the [001]* SAED pattern. If a unidirectional modulation has to be considered, the reflection conditions are consistent with the (3 + 1)-dimensional superspace groups *Immm*(α00)000 and *Immm*(α00)00*s* [13]. Again, in the latter superspace group only reflections *hk*0*m* with $m = 2n$ are allowed explaining the absence of 1st order satellites in the [001]* SAED pattern. As were not able to detect any cross-terms (i.e. satellites attributed to the diffraction vectors $\pm(\mathbf{q}_1 + \mathbf{q}_2)$ or $\pm(\mathbf{q}_1 - \mathbf{q}_2)$) which would definitely prove a two-dimensional modulation, structure models for both cases were developed. The best (3 + 2)-dimensional fit was achieved in superspace group *I*4/*mmm*(0–α0, α00)0.*ss.mm*, whereas in the (3 + 1)-dimensional case the refinement results clearly favor *Immm*(α00)00*s*.

The satellite intensities found in X-ray experiments are in general weak and decrease rapidly with increasing diffraction order: approximately 70% of the 1st-order satellites, but only about 10% of the 2nd-order satellites have intensities above a detection threshold of $3\sigma(I)$; higher-order satellites were not observed. In this context it is

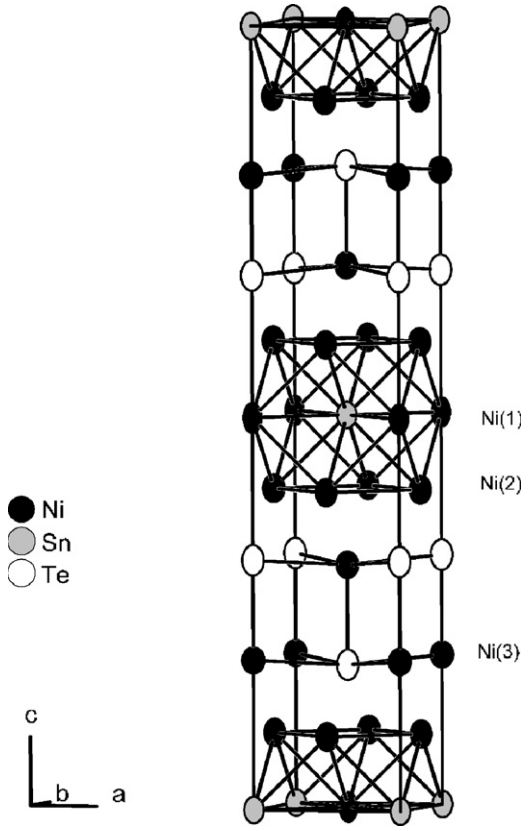

Fig. 2. Average structure, the unit cell is outlined, thermal ellipsoids are given at a probability level of 99.9%, all positions are displayed as fully occupied.

understandable, that no cross-terms—which are all higher-order satellites—were detected. This observation is supported by inspecting the final list of observed (F_o) and calculated (F_c) structure factors after the refinement in superspace group $I4/mmm(0–\alpha0,\ \alpha00)0.ss.mm$: all calculated structure factors of the cross-terms are so small, that not a single F_c exceeds a value of $3\sigma(F_o)$. In other words, there are no observable cross-terms.

The atomic positions of average structure of $Ni_{7-\delta}SnTe_2$ [3] were taken as a starting model for the structure rrefinement. The refinement of the average structure in space group $I4/mmm$ yielded a final residual of $wR_2 = 0.060\%$ for 135 reflections and 17 parameters. The occupancy of Ni(3) (Wyckoff site 4*e*) was computed to 0.395(8) ($\approx 2/5$) pointing towards an occupational modulation of this atom. The overall composition from the refinement of the average structure is $Ni_{5.79(1)}SnTe_2$ and agrees well with the data of a different crystal investigated in [3]. The unit cell of the average structure of $Ni_{7-\delta}SnTe_2$ is depicted in Fig. 2.

Based on the refinement results of the average structure of $Ni_{7-\delta}SnTe_2$, an occupational modulation of Ni(3) could be expected. Physically, an atom can either be present, corresponding to an occupancy of one, or absent with an occupancy of zero. If an incommensurate, but still complete ordering of vacancies and occupied positions of Ni(3) would occur, the occupancy of Ni(3) could best be described by a crenel function, which is defined by only two parameters, its center x_4^0 (x_4 is the atomic coordinates corresponding to the direction of $\mathbf{q}_1$) and its width Δ_p. The occupancy is one for $x_4 = x_4^0 \pm \Delta_p/2$ and zero in all other regions of x_4, cf. Table 8.

Let us first consider the case of a two-dimensional modulation in superspace group $I4/mmm(0–\alpha0,$

Table 2
Crystallographic data for $Ni_{7-\delta}SnTe_2$; (3 + 2)-dimensional structure model

Formula; formula weight; $F(000)$	$Ni_{5.81(1)}SnTe_2$; 715 g/mol; 633
Crystal size	$0.01 \times 0.05 \times 0.09\ mm^3$
Diffractometer	STOE IPDS-2, graphite monochromator, Mo$K\alpha$
Reflections	$-5 \leqslant h,k \leqslant 5$; $-26 \leqslant l \leqslant 26$; $-2 \leqslant m,n \leqslant 2$ $2.1 \leqslant \theta \leqslant 29.3°$; 48,539 reflections collected
Main reflections and satellites	1617 independent, 558 obs. with $I > 3\sigma(I)$
Main reflections only	135 independent, 135 obs. with $I > 3\sigma(I)$
1st-order satellites	461 independent, 344 obs. with $I > 3\sigma(I)$
2nd-order satellites	1021 independent, 79 obs. with $I > 3\sigma(I)$
R_{int}; R_{sigma}	0.083; 0.012
Superspace group; Z	$I4/mmm(0-\alpha0,\ \alpha00)0.ss.mm$; 2
Lattice parameters	$a = 3.759(1)$ Å $c = 19.410(2)$ Å $V = 274.3(1)$ Å^3
Modulation vectors	$\mathbf{q}_1 = (0, -0.410(1), 0)$, $\mathbf{q}_2 = (0.410(1), 0, 0)$
Calc. density; abs. coefficient	8.68 g/cm^3; 34.5 mm^{-1}
Abs. correction	Analytical [5], $T_{min} = 0.03$, $T_{max} = 0.19$
Extinction parameter	0.17(1)
Modulation functions	Harmonic for occupation of Ni(3), site parameters and *adp*'s of Sn, Te, Ni(1), Ni(2), and Ni(3)*
Modulation waves	$1 \cdot \mathbf{q}_1$, $1 \cdot \mathbf{q}_2$, $2 \cdot \mathbf{q}_1$, $2 \cdot \mathbf{q}_2$
Refinement	JANA2000, full matrix against F^2 [4] 47 parameters, no restraints
Weighting scheme	$w = 1/[\sigma^2(I) + 0.0004(I^2)]$
Agreement factors	R_1, w$R_2(I > 3\sigma)$; R_1, wR_2(all I)
Overall	0.043, 0.093; 0.120, 0.108
Main reflections	0.017, 0.053; 0.017, 0.053
1st-order satellites	0.065, 0.106; 0.108, 0.115
2nd-order satellites	0.457, 0.712; 0.497, 0.732
GooF (all I)	1.71
Largest diff. peak/hole	+5.76/–4.22 e/Å^3

*adp: anisotropic displacement parameters.

Table 3
Atomic coordinates, occupancies and coefficients U_{ij} of the tensors of the anisotropic displacement parameter/Å^2 for $Ni_{7-\delta}SnTe_2$; (3 + 2)-dimensional structure model

Atom	Site	Occ.	x	y	z	U_{11}	U_{22}	U_{33}
Sn	2 *a*	1	0	0	0	0.0035(2)	0.0035(2)	0.0064(3)
Te	4 *e*	1	0	0	0.31851(2)	0.0041(2)	0.0041(2)	0.0075(3)
Ni(1)	8 *g*	1	0	$\frac{1}{2}$	0.09408(2)	0.0042(3)	0.0047(3)	0.0070(3)
Ni(2)	2 *b*	1	0	0	$\frac{1}{2}$	0.0036(3)	0.0036(3)	0.0080(4)
Ni(3)	4 *e*	0.405(5)	0	0	0.19074(6)	0.018(2)	0.018(2)	0.023(3)

Table 4
Fourier coefficients S and C of the harmonic modulation function[a] of the site modulation waves (x, y, z) and the occupancy modulation waves (occ) for $Ni_{7-\delta}SnTe_2$; (3 + 2)-dimensional structure model; subscripts 1 and 2 refer to the modulation waves $1 \cdot \mathbf{q}_1$ and $1 \cdot \mathbf{q}_2$, 3 and 4–$2 \cdot \mathbf{q}_1$ and $2 \cdot \mathbf{q}_2$, resp

Atom		x	y	z	Occ
Sn	$S_1 = S_2$	0	0	−0.00082(2)	—
	$C_1 = C_2$	0	0	0	—
Te	S_1	0	0	0.00144(2)	—
	C_1	0	−0.00005(6)	0	—
	S_2	0	0	0.00144(2)	—
	C_2	0.00005(6)	0	0	—
Ni(1)	S_1	0	0	–0.00048(3)	—
	C_1	0	–0.0001(1)	0	—
	S_2	0	0	–0.00072(3)	—
	C_2	0.0001(1)	0	0	—
Ni(2)	$S_1 = S_2$	0	0	–0.00051(4)	—
	$C_1 = C_2$	0	0	0	—
Ni(3)	$S_1 = S_2$	0	0	0	0.374(3)
	C_1	0	–0.0059(4)	0	0
	C_2	0.0059(4)	0	0	0
	$S_3 = S_4$	—	—	—	0
	$C_3 = C_4$	—	—	—	–0.123(4)

[a]The general positional atomic modulation function M is given as a sum of harmonic functions, $M_x(v)$ can be expressed as

$$M_x(v) = \sum_{n=1}^{m} S_{nx} \sin(2\pi nv) + C_{nx} \cos(2\pi nv).$$

Similar expressions are obtained for $M_y(v)$ and $M_z(v)$ and for the occupancy $M_{occ}(v)$, respectively.

α00)0.*ss.mm*. As step-like functions, like the crenel function, are only available for (3 + 1)-dimensional structures in the refinement software, harmonic functions have been used for the fit of the occupancy of Ni(3), as well as of the site parameters and anisotropic displacement parameters of all atoms. The harmonic functions are developed into a truncated Fourier series and Fourier coefficients are used as independent parameters in the refinement (Table 4; for a general definition of the harmonic modulation function in JANA2000, cf. [14]). The number of Fourier coefficients has been limited to two along each modulation direction for the occupancy of Ni(3) and to one for the positional modulation and the modulation function of the displacement parameters for all atoms. No occupancy modulation has been observed for any other atom. Higher-order Fourier coefficients were not used as the refinement suffered from large correlations in these cases. The fit of the occupational modulation of Ni(3) with a truncated Fourier series must be regarded as an approximation which surely leads to over- and undershooting and some truncation effects. The refinement with 47 parameters finally converged to overall agreement factors of $R_1 = 0.043$ and $wR_2 = 0.093$ for 558 reflections classified as observed with $I > 3\sigma(I)$ and $R_1 = 0.120$ and $wR_2 = 0.108$ for all 1617 reflections; the partial residuals for main reflection and satellites can be found in Table 2. The residuals for the second order satellites are quite poor due to their low intensities. The resulting structure model is satisfactory and reasonable interatomic distances are computed. The occupancy of Ni(3) was calculated to 0.405(5), corresponding to a composition of $Ni_{5.81(1)}SnTe_2$. The results of the refinements together with some crystallographic data are given in Tables 2–4, interatomic distances are listed in Table 5. Further details of the crystal structure investigations can be obtained from the Fachinformationszentrum Karlsruhe, 76344 Eggenstein-Leopoldshafen, Germany, (fax: (49) 7247-808-666, e-mail: crysdata@fiz.karlsruhe.de) on quoting the depository number CSD-416331.

Table 5
Selected interatomic distances/Å for $Ni_{7-\delta}SnTe_2$; (3 + 2)-dimensional structure model

Atoms		Ave.	Min.	Max.
Sn–Ni(1)	8 ×	2.621(1)	2.608(1)	2.633(1)
Sn–Ni(2)	4 ×	2.658(1)	2.658(1)	2.658(1)
Te–Ni(1)	4 ×	2.532(1)	2.485(1)	2.581(1)
Te–Ni(3)	1 ×	2.489(1)	2.452(1)	2.536(1)
Te–Ni(3)	4 ×	2.664(1)	2.630(1)	2.699(1)
Ni(1)–Ni(1)	4 ×	2.658(1)	2.657(1)	2.659(1)
Ni(1)–Ni(3)	2 ×	2.658(1)	2.637(2)	2.675(2)
Ni(2)–Ni(1)	8 ×	2.620(1)	2.610(1)	2.631(1)
Ni(3)–Ni(3)	4 ×	3.524(2)	3.485(2)	3.553(2)

Fourier (F_o) sections around the individual atoms can be used to elucidate the effects of the modulation. As we deal with tetragonal 4/*mmm* symmetry, the coordinates x_1 and x_2, as well as x_4 and x_5 are related by symmetry and not too many Fourier sections have to be discussed (x_1, x_2, and x_3 are atomic coordinates corresponding to x, y, and z in a three-dimensional structure, x_4 and x_5 are the atomic coordinates corresponding to the direction of $\mathbf{q}_1$ and $\mathbf{q}_2$). Fig. 3 shows Fourier sections x_4–x_1 around the Ni(3) atom for two different values of x_5 (Fourier sections x_4–x_3 give qualitatively the same results and are thus not presented

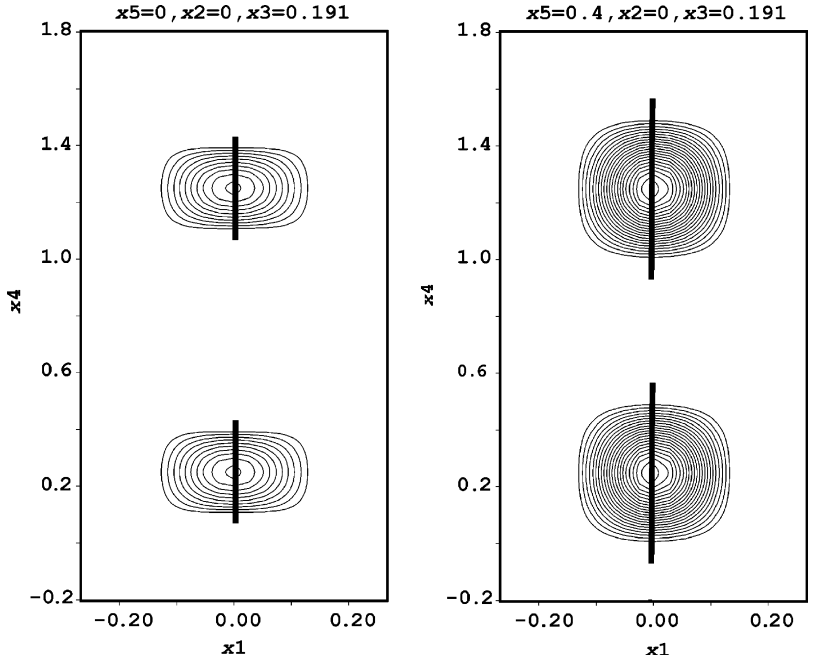

Fig. 3. Fourier-maps (F_o) x_4–x_1 around Ni(3) for $x_5 = 0$ and $x_5 = 0.4$ for the (3 + 2)-dimensional structure model. The electron density is given in steps of 5 e/Å^3; the central fat line indicates the calculated atomic position (occupancy cut-off: 0.35).

here). The Fourier section around a non-modulated atom would look like a rod with its electron density declining symmetrically towards the periphery. This is obviously not the case for Ni(3). The step-like modulation of the electron density can clearly be extracted from Fig. 3. For $x_5 = 0$ and $x_5 = 0.4$ the electron density drops to zero, for example in the basin with $0.5 < x_4 < 1.0$, indicating an ordering of the vacancies. The calculated atomic position (thick central line) follows this behavior. A cut-off value of 0.35 has been chosen for the representation of occupied positions in both figures. The necessity to define an occupancy threshold originates from the harmonic approximation and can be understood by inspecting the occupancy-t-plots (t and u are the internal coordinates corresponding to the modulation vectors $\mathbf{q}_1$ and $\mathbf{q}_2$, respectively; for a definition of t and u cf. [14]). Two of these t-plots are depicted in Fig. 4 for $u = 0$ and $u = 0.4$. For $u = 0$ the calculated occupancy of Ni(3) adopts values close to zero in a large basin with $0.6 \leqslant t \leqslant 0.9$ corresponding to vacancies in these regions. For $u = 0.4$ the curve of the calculated Ni(3) occupancy does not become zero for any value of t, but occupancy minima of approximately 0.3 are computed for the broad hollow with $0.6 \leqslant t \leqslant 0.9$.

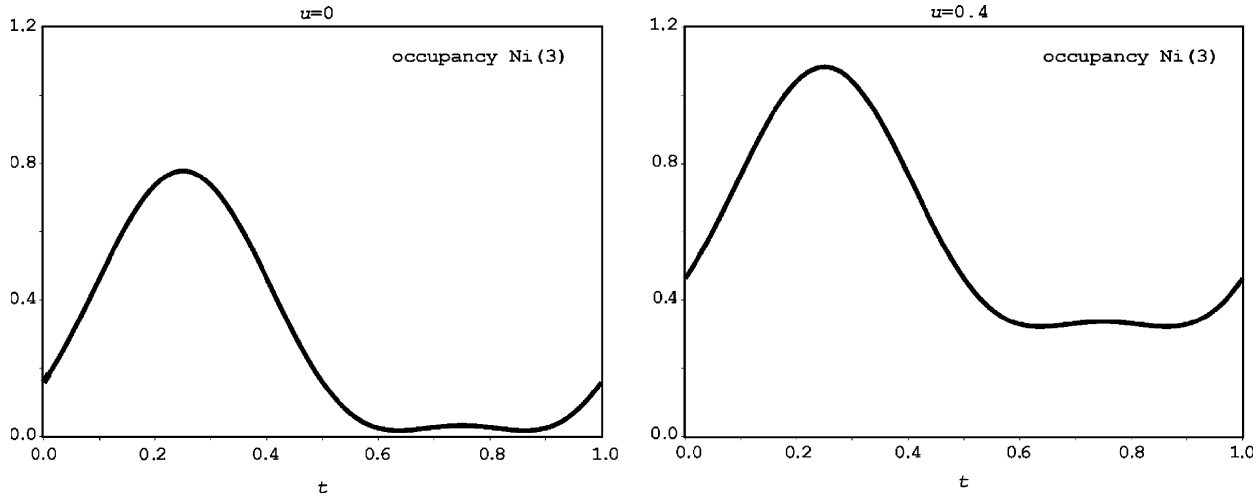

Fig. 4. Occupancy vs. t plot of Ni(3) for $u = 0$ (left) and $u = 0.4$ (right) for the (3 + 2)-dimensional structure model.

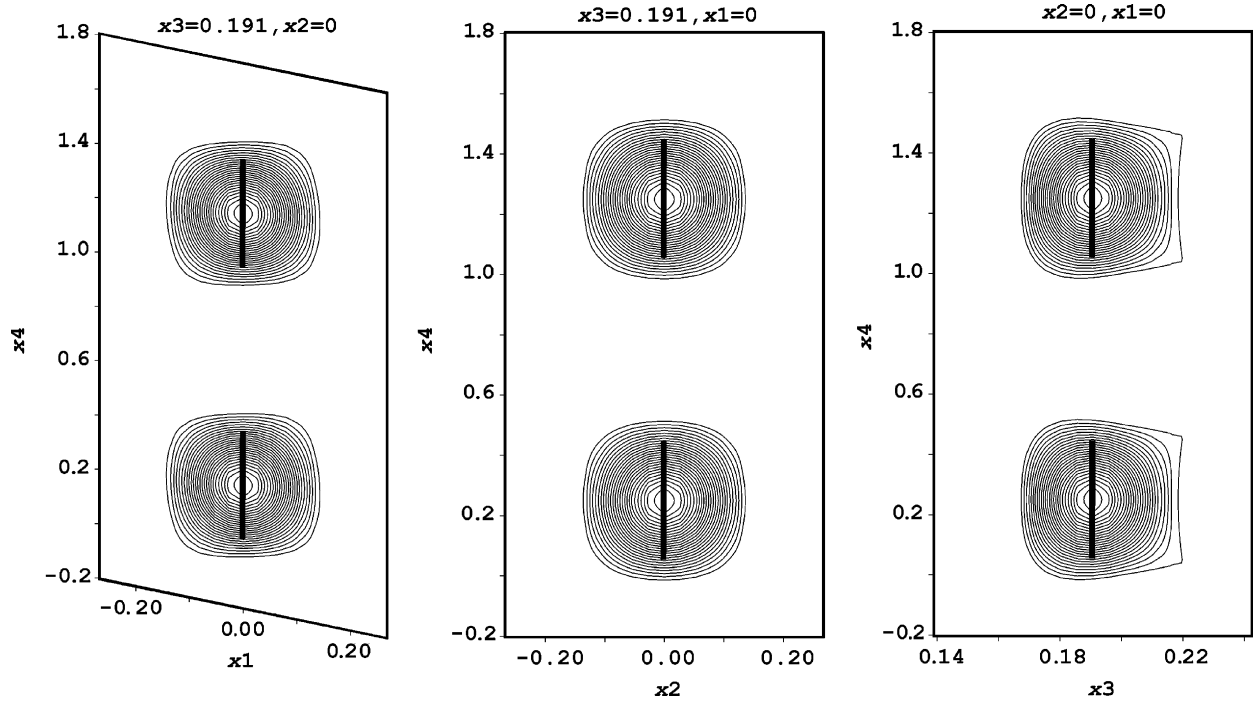

Fig. 5. Fourier-maps (F_o) x_4–x_1, x_4–x_2 and x_4–x_3 around Ni(3) for the (3 + 1)-dimensional structure model. The electron density is given in steps of 5 e/Å^3; the central fat line indicates the calculated atomic position.

As can be seen from the Fourier coefficients of the respective atom sites (Table 4), the amounts of displacement are small for Te and almost not noticeable for Sn, Ni(1) and Ni(2). Hence, the Fourier maps around these atoms do not reveal any further insight and will not be discussed here.

For fitting the structure of $Ni_{7-\delta}SnTe_2$ as a unidirectional modulated orthorhombic structure, the symmetry had to be lowered to *Immm* and the atomic coordinates were transformed accordingly. Due to the symmetry reduction, the position of Ni(1) (Wyckoff site 8 *g* in *I*4/*mmm*) has to be splitted into two fourfold positions (Wyckoff site 4*j*), which were labeled Ni(1a) and Ni(1b) so that the atoms showing the occupancy modulation are Ni(3) again. In order to reduce correlations it was necessary to set some restrictions concerning the Ni atoms: z of Ni(1b) was fixed to $-z$ of Ni(1a) and the U_{11} and U_{22} for all Ni atoms were set to equal values. The refinement of the basic structure in space group *Immm* then converged to final residual of $wR_2 = 0.083\%$ for all 242 reflections and 21 parameters. The occupancy of Ni(3) was computed to 0.411(9), the overall composition from the refinement of the average structure is $Ni_{5.82(1)}SnTe_2$ in this case.

As stated before, the (3 + 1)-dimensional structure could best be fitted in superspace group *Immm*(α00)00*s*. As a start, a crenel function for the occupancy modulation was introduced for Ni(3), since a positional modulation for this atom is negligible. Due to large correlations, the center of the crenel function has been fixed to $x_4^0 = 0.25$ after inspection of the respective Fourier maps (Fig. 5); the restrictions which were necessary for the refinement of the 3D basic structure could on the other hand be eliminated. Subsequently, harmonic modulation functions with first order Fourier coefficients were brought in for the positional modulation of Sn, Te, Ni(1a), Ni(1b) and Ni(2) and for the anisotropic displacement parameters of

Table 6
Crystallographic data for $Ni_{7-\delta}SnTe_2$; (3 + 1)-dimensional structure model

Formula; formula weight; *F*(000)	$Ni_{5.79(1)}SnTe_2$; 714 g/mol; 632
Crystal size	$0.01 \times 0.05 \times 0.09\ mm^3$
Diffractometer	STOE IPDS-2, graphite monochromator, Mo*K*α
Reflections	$-5 \leqslant h,k \leqslant 5$; $-26 \leqslant l \leqslant 26$; $-2 \leqslant m \leqslant 2$ $2.1 \leqslant \theta \leqslant 29.3°$; 9742 reflections collected
Main reflections and satellites	1089 independent, 589 obs. with $I > 3\sigma(I)$
Main reflections only	243 independent, 243 obs. with $I > 3\sigma(I)$
1st-order satellites	412 independent, 289 obs. with $I > 3\sigma(I)$
2nd-order satellites	434 independent, 57 obs. with $I > 3\sigma(I)$
R_{int}; R_{sigma}	0.070; 0.004
Superspace group; *Z*	*Immm*(α00)00*s*; 2
Lattice parameters	$a = 3.759(1)$ Å $b = 3.759(1)$ Å $c = 19.410(2)$ Å $V = 274.3(1)$ Å^3
Modulation vector	$\mathbf{q}_o = (0.410(1), 0, 0)$
Calc. density; abs. coefficient	8.65 g/cm^3; 34.2 mm^{-1}
Abs. correction	Analytical [5], $T_{min} = 0.04$, $T_{max} = 0.21$
Extinction parameter	0.37(1)
Modulation functions	Crenel function for occupation of Ni(3), harmonic function for site parameters of Sn, Te, Ni(1a), Ni(1b), Ni(2) and *adp*'s of Sn and Te[a]
Modulation waves	$1 \cdot \mathbf{q}_o$, $2 \cdot \mathbf{q}_o$
Refinement	JANA2000, full matrix against F^2 [4] 39 parameters, no restraints
Weighting scheme	$w = 1/[\sigma^2(I) + 0.0009(I^2)]$
Agreement factors	R_1, $wR_2(I > 3\sigma)$; R_1, wR_2(all *I*)
Overall	0.038, 0.102; 0.063, 0.111
Main reflections	0.029, 0.087; 0.029, 0.087
1st-order satellites	0.038, 0.073; 0.082, 0.087
2nd-order satellites	0.529, 0.788; 0.505, 0.796
GooF (all *I*)	1.88
Largest diff. peak/hole	+5.32/−3.65 e/Å^3
Twin matrix; twin volumes	(010, 100, 001); 0.37(1)/63

[a] *adp*: anisotropic displacement parameters.

Table 7
Atomic coordinates, occupancies and coefficients U_{ij} of the tensors of the anisotropic displacement parameter/Å^2 for $Ni_{7-\delta}SnTe_2$; (3 + 1)-dimensional structure model

Atom	Site	Occ.	*x*	*y*	*z*	U_{11}	U_{22}	U_{33}
Sn	2 *a*	1	0	0	0	0.0024(7)	0.0055(8)	0.0061(4)
Te	4 *i*	1	0	0	0.31844(2)	0.0025(5)	0.0075(6)	0.0072(3)
Ni(1a)	4 *j*	1	0	$\frac{1}{2}$	0.0940(1)	0.0033(9)	0.0046(9)	0.0088(5)
Ni(1b)	4 *j*	1	0	$\frac{1}{2}$	−0.0944(1)	0.0044(9)	0.0046(9)	0.0040(5)
Ni(2)	2 *c*	1	0	0	$\frac{1}{2}$	0.0038(12)	0.0024(11)	0.0065(5)
Ni(3)	4 *i*	0.394(3)	0	0	0.19074(8)	0.0033(7)	0.0038(8)	0.0067(7)

Table 8
Fourier coefficients *S* and *C* of the harmonic modulation function[a] of the site modulation waves (*x*, *y*, *z*) for Sn, Te, Ni(1a), Ni(1b) and Ni(2) and crenel parameters (center, x_4^0, and width, Δ_p) of the occupancy modulation (occ) waves for $Ni_{7-\delta}SnTe_2$; (3 + 1)-dimensional structure model; subscript 1 refers to the modulation waves $1 \cdot \mathbf{q}$

Atom		*x*	*y*	*z*	Occ
Sn	S_1	0	0	–0.00142(5)	—
	C_1	0	0	0	—
Te	S_1	0	0	0.00235(4)	—
	C_1	0.0019(1)	0	0	—
Ni(1a)	S_1	0	0	–0.00128(6)	—
	C_1	0.0070(3)	0	0	—
Ni(1b)	S_1	0	0	–0.00065(6)	—
	C_1	–0.0017(3)	0	0	—
Ni(2)	S_1	0	0	–0.00049(9)	—
	C_1	0	0	0	—
Ni(3)	x_4^0	–	—	—	0.25
	Δ_p	–	—	—	0.394(3)

The crenel function *pv* for the occupancy modulation is defined as

$$p_v(x_4) = 1 \quad x_4 \in \langle x_4^0 - \Delta_p/2, x_4^0 - \Delta_p/2 \rangle,$$

$$p_v(x_4) = 0 \quad x_4 \notin \langle x_4^0 - \Delta_p/2, x_4^0 - \Delta_p/2 \rangle.$$

[a] For the harmonic modulation function *M* cf. Table 4.

Sn and Te. The refinement with 39 parameters converged to overall agreement factors of $R_1 = 0.038$ and $wR_2 = 0.102$ for 589 reflections classified as observed with $I > 3\sigma(I)$ and $R_1 = 0.063$ and $wR_2 = 0.111$ for all 1089 reflections; the partial residuals for main reflection and satellites can be found in Table 6. The (3 + 1)-dimensional structure model is also satisfactory and gives reasonable interatomic distances. The occupancy of Ni(3) was calculated to 0.394(3), corresponding to the formula $Ni_{5.79(1)}SnTe_2$. The twin ratio was refined to 0.37(1): 0.63. The results of the refinements together with some crystallographic data are given in Tables 6–8; interatomic distances are listed in Table 9.

Table 9
Selected interatomic distances/Å for $Ni_{7-\delta}SnTe_2$; (3 + 1)-dimensional structure model

Atoms		Ave.	Min.	Max.
Sn–Ni(1a)	4 ×	2.619(2)	2.617(2)	2.621(2)
Sn–Ni(1b)	4 ×	2.624(2)	2.610(2)	2.639(2)
Sn–Ni(2)	4 ×	2.658(1)	2.658(1)	2.658(1)
Te–Ni(1a)	2 ×	2.535(2)	2.504(2)	2.566(2)
Te–Ni(1b)	2 ×	2.530(1)	2.491(2)	2.569(2)
Te–Ni(3)	1 ×	2.514(2)	2.496(2)	2.524(2)
Te–Ni(3)	4 ×	2.667(2)	2.662(1)	2.670(2)
Ni(1a)–Ni(1b)	4 ×	2.658(1)	2.640(1)	2.676(1)
Ni(1a)–Ni(3)	2 ×	2.671(1)	2.644(2)	2.675(2)
Ni(1b)–Ni(3)	2 ×	2.651(2)	2.642(2)	2.660(2)
Ni(2)–Ni(1a)	2 ×	2.619(2)	2.599(2)	2.639(2)
Ni(2)–Ni(1b)	2 ×	2.624(2)	2.622(2)	2.626(2)
Ni(3)–Ni(3)	4 ×	3.515(2)	3.515(2)	3.515(2)

Fourier sections x_4–x_1, x_4–x_2 and x_4–x_3 around the Ni(3) atom are depicted in Fig. 5. The discontinuous modulation of the electron density is fitted suitably by the crenel function, although in this case a slight undershooting of the calculated position has to be stated. The slight anisotropy of the electron density distribution along x_3 originates from a small displacement of the Ni(3) atom in the crystallographic c-direction. The t-plot of the occupancy is shown in Fig. 6. The occupancy of Ni(3) is one in the interval $0.05 \leqslant t \leqslant 0.45$ and zero for all other values of t. Overall, the occupancy-t-plot is comparable with the t-plots for the (3 + 2)-dimensional case (Fig. 4). The amounts of displacement are again small for Te and almost not noticeable for Sn, Ni(1a/b) and Ni(2); the Fourier maps around these atoms will not be discussed here.

Since the effects of the modulation are hardly visible in any projection of the unit cell content along the

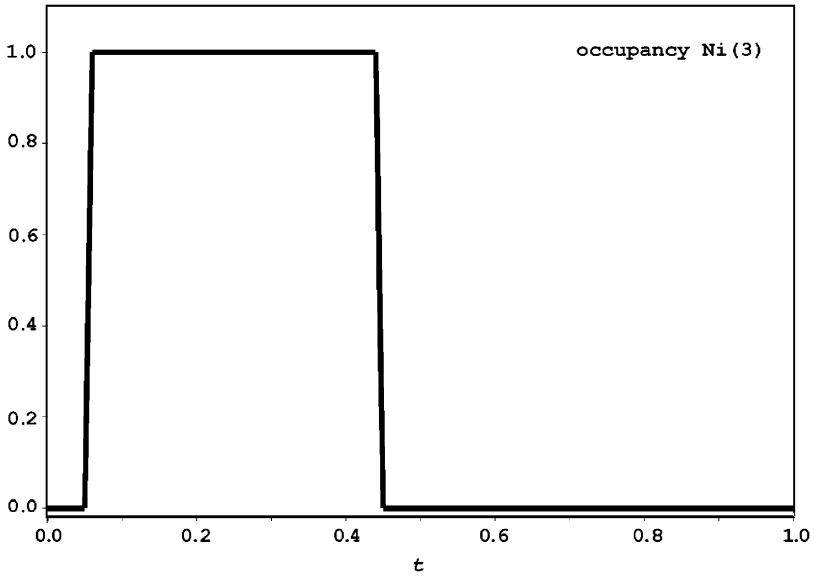

Fig. 6. Occupancy vs. t plot of Ni(3) for the (3 + 1)-dimensional structure model.

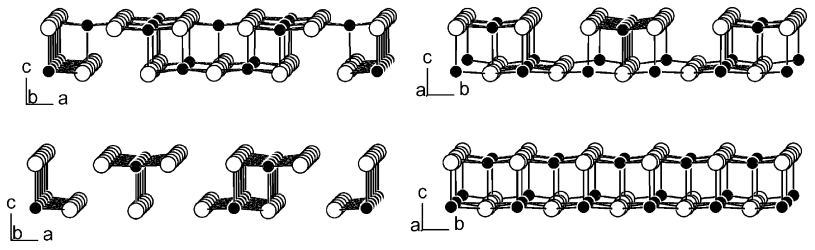

Fig. 7. Section of the Ni(3)/Te slab of the modulated structure of $Ni_{7-\delta}SnTe_2$ seen along [010] (left) and [100] (right); top: (3 + 2)-dimensional model, bottom: (3 + 1)-dimensional model; Ni atoms as black, Te atoms as white circles.

crystallographic axes, an arbitrary view of a section of one Ni(3)/Te slab was chosen to elucidate the modulation results. The modulated structure as a result of the tetragonal model in $I4/mmm(0–\alpha0, \alpha00)0.ss.mm$ is depicted in the top of Fig. 7, the respective section calculated with the orthorhombic structure in $Immm(\alpha00)00s$ is given at the bottom of the figure. The images were calculated covering six times the basic lattice parameters a and b and, thus, more than one modulation period along $\mathbf{q}_1$ and $\mathbf{q}_2$. A cut-off value for the occupancy of 0.56 for the representation of occupied Ni(3) positions has been taken for the image resulting from the (3 + 2)-dimensional fit, representing a composition of $Ni_{5.82}SnTe_2$. In the one dimensionally modulated case, no cut-off value is needed since only occupancies of 1 or 0 occur. The starting assumption for the refinement of the (3 + 1)- and (3 + 2)-dimensional modulated structures are quite different, however, the resulting structure models are fairly similar. This can structurally be understood as a result of the tetragonal symmetry of the average structure and the arrangement of Ni(3) in a square net. The absence of atoms along one direction in the square net necessarily produces vacancies in the direction perpendicular to it. We take this as a further indication that the description of the structure of $Ni_{5.81}SnTe_2$ as a two-dimensionally modulated one is appropriate. The fit as unidirectional modulation results in either fully occupied or empty rows of Ni(3) along the viewing direction. In the bidirectional modulated case, fully and partially occupied rows of Ni(3) and empty channels can be seen. Looking down [100], the image of the tetragonal modulated model remains more or less the same as seen along [010], which is not unexpected regarding the $4/mmm$ symmetry. The orthorhombic model produces a slightly different image: only partially occupied rows of Ni(3) atoms, but no empty channels occur in this case.

Neither the diffraction data, nor the refinement results for the modulated structures rule out or definitely confirm one of the two possible structure models for $Ni_{7-\delta}SnTe_2$. However, based on the results for the analogous compound $Pd_{7-\delta}SnTe_2$ [4] we chose the tetragonal (3 + 2)-dimensional model $Ni_{5.81}SnTe_2$ for the following final structure description and the discussion of the interatomic distances and coordination spheres.

The occurrence of vacancies on Ni(3) positions is obviously the major contribution to the modulation. The positional modulation of the all atoms is comparatively

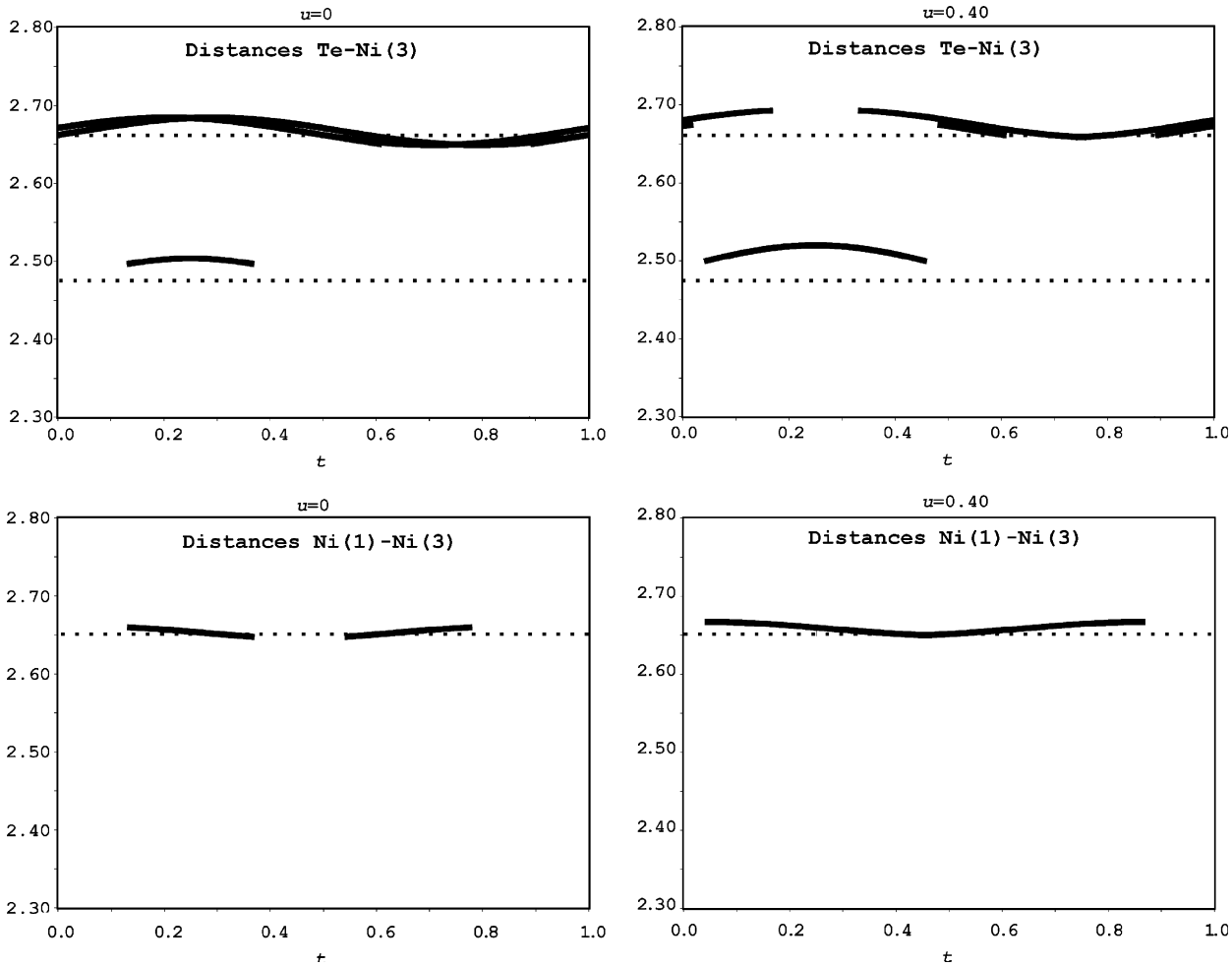

Fig. 8. t plot for the Ni(3)–Te and Ni(3)–Ni(1) distances; (3 + 2)-dimensional structure model.

small as can be read out from the respective Fourier coefficients in Table 4. The Te atoms, the nearest neighbors of Ni(3) in the Ni/Te slabs and, to a lesser extend, the Ni(1) atoms, the nearest neighbors in the heterometallic $^{2}_{\infty}[Ni_5Sn]$ stacks, react in response to the emerging vacancies. The positions of these atoms are slightly modulated, the largest shifts are found along [001]. The Sn and Ni(2) atoms are quite far from the vacancies and remain nearly unaffected. Surprisingly, the interatomic distances Ni(3)–Te and Ni(3)–Ni(1) do not vary much along t and u, respectively (Fig. 8).

The two different Ni(3)–Te distances of 2.489 (1 ×) and 2.664 Å (4 ×) in the average structure alter between 2.452 and 2.536 Å and between 2.630 and 2.699 Å in the modulated phase, giving a variation (Δ) of only about 3%. Due to the occupancy modulation of Ni(3), a reduction of the number of nearest neighbors around Te in some regions of the modulated phase occurs, and less than five Ni(3)–Te distances are found then. For comparison: the respective Pd(3)–Te distance intervals in the homologous modulated structure of $Pd_{6.21}SnTe_2$ are 2.501–2.693 Å for the shorter contact and 2.766–2.936 Å for the longer distances. The percentage of variation for the distances is roughly twice as much here, approximately 6–7%. The distances in the average structure of $Pd_{6.21}SnTe_2$ are 2.580 Å (1 ×) and 2.853 Å (4 ×). The Ni(3)–Ni(1) distances in the modulated structure of the title compound range from 2.637 to 2.675 Å ($\Delta = 1.5\%$), the respective distances in the average structure are 2.658 Å ($Pd_{6.21}SnTe_2$: Pd(3)–Pd(1) distances: 2.917–2.986 Å; $\Delta = 2.3\%$). The Te–Ni(1) distances fall into the range from 2.485 to 2.581 Å ($\Delta = 3.8\%$) and are thus somewhat shorter than the four Te–Ni(3) distances in the Ni/Te slabs ($Pd_{6.21}SnTe_2$: Te–Pd(1) distances: 2.642–2.734 Å; $\Delta = 3.3\%$). The Te–Ni(1) distances in the average structure are 2.532 Å. The modulation has little influence on the Sn/Ni slab. The Sn–Ni(2) distances remain unaffected (2.658 Å; average structure: 2.658 Å), and the alterations in the Sn–Ni(1) distances (2.608–2.633 Å, $\Delta = 1\%$; average structure: 2.621 Å) are small. Similar minute extents of the variation were determined for the respective Sn–Pd distances in $Pd_{6.21}SnTe_2$: Sn–Pd(2) = 2.829 Å, Sn–Pd(1) = 2.779–2.835 Å ($\Delta = 2\%$).

3.2. Electronic structure and bonding

As the modulated crystal structure cannot be taken as a basis for band structure calculations, a fourfold commensurate superstructure based on the composition $Ni_{5.75}SnTe_2$ (corresponding to s.o.f = 0.375 for Ni(3) in the average structure) was chosen as approximant [3]. The space group and lattice parameters of that model are: $Cmmm$, $a = b = 10.6575$ Å, $c = 19.419$ Å.

The calculated band structure of $Ni_{5.75}SnTe_2$ in the vicinity of the Fermi level is shown in Fig. 9. A strong anisotropy of the band structure in M–Γ–X (crystallographic ab plane) vs. Γ–Z directions (crystallographic c direction) is evident as can be seen from the different band dispersions and the number of bands crossing the Fermi level along both directions. The higher is the number of bands crossing the Fermi level in a certain direction, the more electronic states with the energy close to the Fermi energy exist. Since the conductivity is proportional to the number of electronic states near the Fermi level, the anisotropy of the electroconductivity is evident.

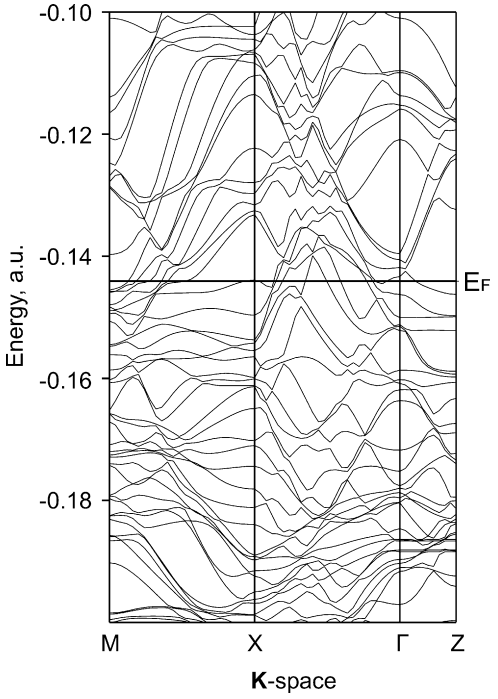

Fig. 9. Calculated band structure of the commensurate approximant $Ni_{5.75}SnTe_2$.

The calculated curves of the density of states (DOS) are shown in Fig. 10. All atomic states are strongly mixed; no DOS peaks have a dominant contribution from only one atom type. Disregarding the difference in coordination, it can be noted, that the states of nickel atoms from the heterometallic slabs are located in essentially the same energy range as those from the nickel-chalcogenide slabs. The states in the vicinity of the Fermi level mainly originate from Ni d-orbitals from the heterometallic slabs. A similar picture was previously observed for nickel–tin sulfides [2] and selenide [3].

3.3. Electrical properties

The temperature dependence of the resistivity measured parallel ($\rho_{\parallel}$) and orthogonal ($\rho_{1\perp}$ and $\rho_{2\perp}$) to the crystallographic c direction is shown in Fig. 11 in a semi-logarithmic scale. As can be seen from the figure, the crystal shows metallic conductivity and the value of $\rho_{\parallel}$ is significantly larger than $\rho_{1\perp}$ and $\rho_{2\perp}$ in the whole temperature interval, while the values of $\rho_{1\perp}$ and $\rho_{2\perp}$ are in the same magnitude. The electrical current flowing through the edge of the crystal only reduces the observed

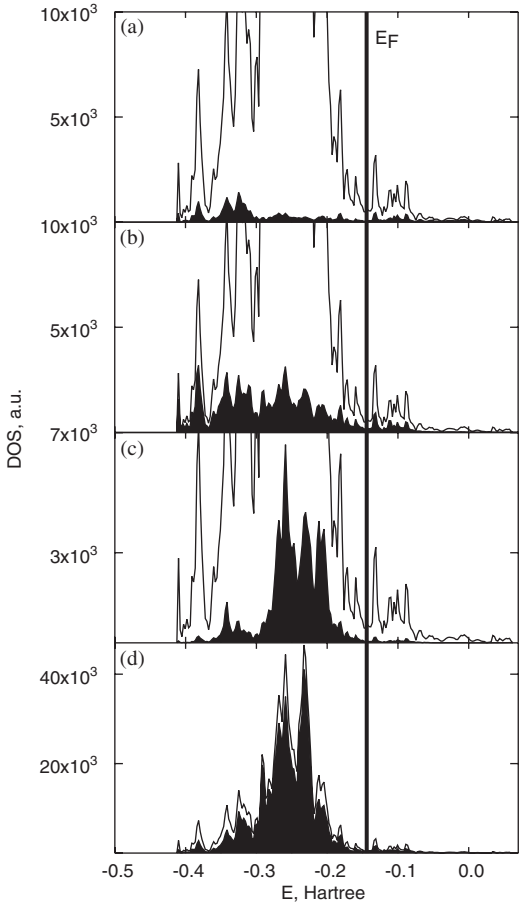

Fig. 10. Total and partial DOS curves for $Ni_{5.75}SnTe_2$ (commensurate approximant): (a) Sn; (b) Te; (c) Ni in $^2_\infty[Ni_{0.75}Te_2]$; (d) Ni in $^2_\infty[Ni_5Sn]$.

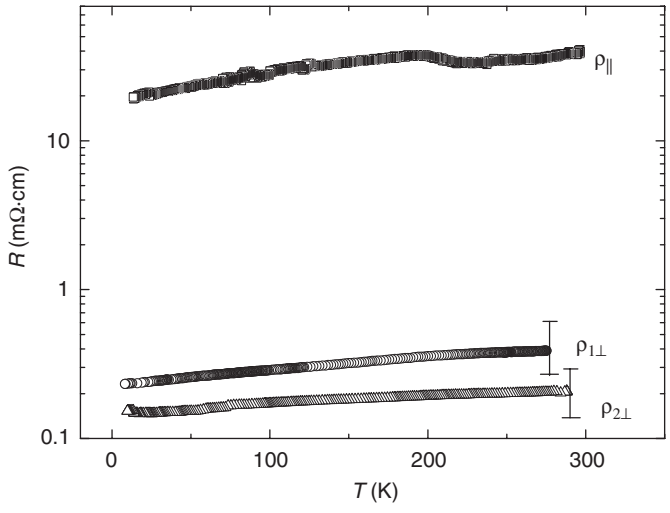

Fig. 11. Temperature dependence of the resistivity parallel ($\rho_\parallel$) and orthogonal ($\rho_\perp$) to the c axis (single crystal data).

value of the resistance anisotropy $\rho_\perp/\rho_\parallel$. The accuracy of the measurements of the in-plane resistivity is shown by error margins for one single value of resistivity (Fig. 11). For resistivity measurements along c-axis direction, the experimental error is about the size of the symbol in figure. The error is mainly caused by geometrical factors arising from the shape of the crystal.

Since X-ray investigations showed, that the modulated structure remains unchanged in the temperature interval between 153 and 293 K, the peculiarity in the resistivity curve $\rho_\parallel$ at $T \approx 220$ K is not connected to a phase transition. It may be caused by a shift of the chemical potential in the conduction band due to temperature change near the feature of the DOS.

The anisotropy $\rho_\perp/\rho_\parallel$ of the electroconductivity is caused by the anisotropy of the crystal structure and the quasi two-dimensional character of the band structure (Fig. 9). Hall effect measurements revealed that the electron concentration in the sample is $\geqslant 10^{21}$ cm^{-3}, which is typical for metals.

4. Conclusion

The refined modulated structure of $Ni_{5.81}SnTe_2$ resembles some structural features of $Ni_{2.76}Te_2$. The orthorhombic modification of the non-stoichiometric nickel telluride, a distorted variant of the Cu_2Sb type, was stabilized at room temperature by incorporation of about 10% of iron (prepared as $Ni_{2.57}Fe_{0.29}Te_2$). Its modulated structure was refined in superspace group $Pmmn(a00)0s0$, with lattice parameters $a = 3.761(1)$, $b = 3.796(1)$, $c = 6.084(4)$ Å and a modulation vector $\mathbf{q} = 0.378(1)a^*$ using occupational and displacive modulation functions [15]. The structure of $Ni_{5.81}SnTe_2$ can virtually be generated from that of $Ni_{2.76}Te_2$ by insertion of flat, checkerboard-like [NiSn] layers between adjacent layers of [Ni_5] pyramids in $Ni_{2.76}Te_2$ followed by a shift of two contiguous layers of [Ni_5] pyramids relative to each other by a value of $a/2$, Fig. 12. The occupational modulations in $Ni_{5.81}SnTe_2$ and $Ni_{2.76}Te_2$ affect similar sites on the top of nickel square pyramids and the modulation vectors of both compounds are comparable.

The binary copper telluride $Cu_{2.91}Te_2$ also crystallizes in a Cu_2Sb-based type incommensurately modulated structure [16], where in general the same occupational modulation of the d-metals (Cu) occurs. But unlike $Ni_{2.76}Te_2$, the copper compound reveals an antiphase ordering along the crystallographic c-axis and a different displacement pattern of the modulated Cu atoms. It seems thus reasonable that mixed copper–p-metal chalcogenides with structure analogous to that of the title compound might be expected. This discussion cannot be expanded on palladium compounds as no isostructural non-stoichiometric binary palladium tellurides with modulated structures are known to date.

Neither Ni_3Se_2 nor Ni_3S_2, both crystallizing in the Ni_3S_2 structure type, resemble $Ni_{2.76}Te_2$-like modulated structures. However, the structures of the respective ternary compounds Ni_6SnS_2 [2] and $Ni_{5.62}SnSe_2$ [3] reveal the same structural arrangement of nickel-chalcogenide slabs sandwiched by flat heterometallic [NiSn] layers as observed in repeats the structural motive of $Ni_{2.76}Te_2$.

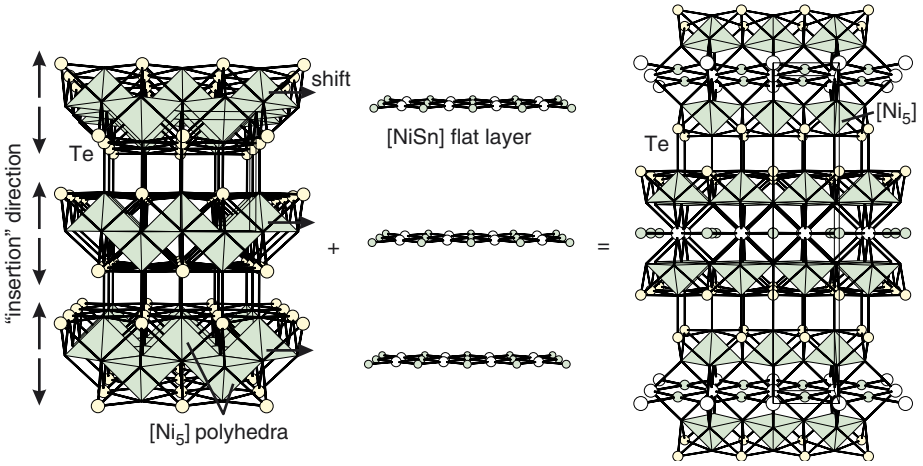

Fig. 12. Structural relationship between $Ni_{2.76}Te_2$ (left) and $Ni_{5.81}SnTe_2$ (right).

The type of modulation observed in the structure of $Ni_{5.81}SnTe_2$ appears to be the same as in the previously reported modulated structure of $Pd_{6.21}SnTe_2$ [4]. The directions of the modulation vectors of both compounds are identical, their lengths are very similar. Both modulated structures can be described in the (3 + 2)-dimensional superspace group $I4/mmm(0–\alpha0,\ \alpha00)0.ss.mm$. In both structures modulation waves occur due to the ordering of *d*-metal atoms over partially occupied sites within metal-telluride slabs. The effects of the modulation on interatomic distances are more pronounced for the Pd compound. The occupation of the *M* positions (Wyckoff site 4*e*) in the $[M_xCh_2]$ slabs is slightly different for both compounds: about 0.6 for $Pd_{6.21}SnTe_2$ and 0.4 for $Ni_{5.81}SnTe_2$. Taking the average structure of $Ni_{5.62}SnSe_2$ [3] into account, yet another occupancy (0.3) has to be considered. It is however not clear to us, what exactly governs the occupancy of the isostructural—at least as far as the average structures are concerned—compounds. The fact that the *d*-metal content of the nickel compounds is slightly lower than that of the palladium compound and that the nickel–tin selenide has a lower *d*-metal content than the tellurides may suggest an influence of the size of the atoms involved. However to clarify this is, amongst others, a task for further investigations. The partial occupancy of Ni(3) site is observed for all non-stoichiometric ternary chalcogenides of this family. It is as well possible, that the structures of some ternary sulfides and selenides are modulated, too, since we observed additional weak reflections in X-ray powder diagrams of phase pure $Ni_{5.62}SnSe_2$ which could not be indexed in a tetragonal unit cell or in simple supercells [3]. The question, whether the same kind of modulation is a common feature for all members of the structure family under consideration, should also be a matter of future studies.

Acknowledgments

This work was supported by Russian Foundation for Basic Research (Grant No. 06-03-32798-a) and by the program of RAS (Russian Academy of Science) Presidium (Grant No. 8P15). The authors thank Dr. A. M. Abakumov for the fruitful discussion.

Supporting information available

X-ray crystallographic files for $Ni_{5.81}SnTe_2$ (CIF). Basis set and input coordinates used in the calculations of electronic structure with the CRYSTAL98 software.

References

[1] T.K. Reynolds, J.G. Bales, F.J. Di Salvo, Chem. Mater. 14 (2002) 4746.
[2] A.I. Baranov, A.A. Isaeva, L. Kloo, B.A. Popovkin, Inorg. Chem. 42 (2003) 6667.
[3] A.I. Baranov, A.A. Isaeva, L. Kloo, V.A. Kulbachinskii, R.A. Lunin, V.N. Nikiforov, B.A. Popovkin, J. Solid State Chem. 177 (2004) 3616.
[4] S.V. Savilov, A.N. Kuznetsov, B.A. Popovkin, V.N. Khrustalev, P. Simon, J. Getzschmann, Th. Doert, M. Ruck, Z. Anorg. Allg. Chem. 631 (2005) 293.
[5] X-AREA, IPDS Software package, STOE STOE & Cie., 2006.
[6] X-RED: Program for Data Reduction and Absorption Correction, STOE & Cie., Darmstadt, 2001; X-SHAPE: Crystal Optimisation for Numerical Absorption Correction, STOE & Cie., Darmstadt, 1999.
[7] V. Petricek, M. Dusek, JANA2000, Crystallographic Computing System, Prague, 2002.
[8] P.J. Becker, P. Coppens, Acta Crystallogr. A 30 (1974) 129; P.J. Becker, P. Coppens, Acta Crystallogr. A 30 (1974) 148.
[9] DIAMOND, Visual Crystal Information System, Crystal Impact GbR, Bonn, 2005.
[10] V.R. Saunders, R. Dovesi, C. Roetti, M. Causa', N.M. Harrison, R. Orlando, C.M. Zicovich-Wilson, CRYSTAL98 User's Manual, University of Torino, Torino, 1998.
[11] (a) for Ni: F. Freyria-Fava, Thesis, Turin, 1997; (b) for Sn, Te: P.J. Hay, W.R. Wadt, J. Chem. Phys. 82 (1) (1985) 284.
[12] (a) A.D. Becke, J. Chem. Phys. 98 (1993) 5648; (b) C. Lee, W. Yang, R.G. Parr, Phys. Rev. B 37 (1988) 785.
[13] A. Yamamoto, Acta Crystallogr. A 52 (1996) 509.
[14] V. Petricek, M. Dusek, JANA98 User's Manual, Prague, 2000; M. Dusek, V. Petricek, K. Fejfarova, L. Palatinus, JANA2000 User's Manual, Prague, 2003.
[15] W.J. Schutte, J.L. de Boer, Acta Crystallogr. B 49 (1993) 392.
[16] W.J. Schutte, J.L. de Boer, Acta Crystallogr. B 49 (1993) 398.